EXPERIMENTAL AND NUMERICAL THERMO – MECHANICAL ANALYSIS OF FRICTION STIR WELDING OF HIGH – STRENGTH ALLUMINIUM ALLOY

by

Darko M. VELJIĆ[a], Aleksandar S. SEDMAK[b*,*], Marko P. RAKIN[c], Nikola S. BAJIĆ[a], Bojan I. MEDJO[c], Darko R. BAJIĆ[d], and Vencislav K. GRABULOV[e]

[a] IHIS Techno Experts Ltd., Belgrade, Serbia
[b] Faculty of Mechanical Engineering, University of Belgrade, Belgrade, Serbia
[c] Faculty of Technology and Metallurgy, University of Belgrade, Belgrade, Serbia
[d] Faculty of Mechanical Engineering, University of Montenegro, Montenegro
[e] Institute for Materials Testing IMS, Belgrade, Serbia

Original scientific paper
DOI: 10.2298/TSCI130512171V

This paper presents experimental and numerical analysis of the change of temperature and force in the vertical direction during the friction stir welding of high-strength aluminium alloy 2024 T3. This procedure confirmed the correctness of the numerical model, which is subsequently used for analysis of the temperature field in the welding zone, where it is different to determine the temperature experimentally. 3D finite element model is developed using the software package Abaqus; arbitrary Lagrangian-Eulerian formulation is applied. Johnson-Cook material law and Coulomb's Law of friction are used for modelling the material behaviour.

Temperature fields are symmetrical with respect to the welding line. The temperature values below the tool shoulder, i. e. in the welding zone, which are reached during the plunge stage, are approximately constant during the entire welding process and lie within the interval 430-502 °C. The temperature of the material in the vicinity of the tool is about 500 °C, while the values on the top surface of the welding plates (outside the welding zone, but close to the tool shoulder) are about 400 °C. The temperature difference between the top and bottom surface of the plates is small, 10-15 °C.

Key words: *friction stir welding, aluminium alloys, finite element analysis, temperature fields, thermo-vision measurement*

Introduction

Friction stir welding (FSW) is a solid-state joining technique invented and patented in 1991 by The Welding Institute (TWI) at Cambridge, UK. It enables the joining of metallic materials which cannot easily (or at all) be joined by conventional welding techniques. FSW is a process of joining in the solid state, and it combines the action of heat and mechanical work [1-3]. Majority of metals suitable for this welding technique are light metals and alloys; most often of them is aluminium, which is characterized by good corrosion resistance, good stiffness-to-weight ratio and strength-to-weight ratio. Aluminium parts with thickness of up to

* Corresponding author, e-mail: asedmak@mas.bg.ac.rs

50 mm can be joined by FSW in single-sided joint, while two-sided joints are needed for thickness of up to 75 mm [2]. In addition to aluminium alloys, materials which can be joined include copper and alloys, lead, titanium and alloys, magnesium alloys, zinc, soft steels, stainless steels, nickel alloys, *etc*. Also, similar and dissimilar materials can be welded by FSW. Regarding the geometry, it can be used for plates, sheets, cylindrical parts, assemblies, *etc*. Friction stir welding process is complex and nonlinear, and it is accompanied by large plastic deformation, high temperatures and plastic flow of the material in the welding zone. The welding zone, which is often categorized as the thermo-mechanically influenced zone due to the complex thermo-mechanical state, is mostly in plastic state (*i. e.* with high level of plastic deformation) and it is difficult to determine the temperatures in it experimentally. Analysis of the complex thermo-mechanical conditions during the welding process in this zone can contribute to a better control of the process. Modelling of the FSW has a key role in the development process and decrease of the experimental expenses. The models provide the information needed for optimization and qualification of the current and future applications of the FSW process [4-13]. In order to justify the thermo-mechanical model, the correlation of experimental and numerical results (regarding the temperature and vertical force) is analysed in this work.

Experiment

The work pieces (plates to be welded) were produced from aluminium alloy 2024 T3, with thickness 3 mm. The dimensions of the sheets are 180 × 65 × 3 mm. Chemical composition of 2024-T3 aluminium: Cu - 4.80, Mg - 1.41, Mn - 0.72, Fe - 0.28, Si - 0.13, Zn - 0.07, Ti – 0.15, other, total - 0.03 %, Al - balance, in accordance with [14]. The thermal and mechanical properties of this alloy, which are used for the numerical model, are given in tab. 1.

Table 1. Material properties of EN AW 2024 T3 [14,15]

Material properties	Value
Young's modulus *E* [GPa]	73.1
Poisson´s ratio *v* [-]	0.33
Thermal conductivity *k* [W/m°C]	121
Coefficient of thermal expansion [°C^{-1}]	24.7x10^{-6}
Density [kg/m^3]	2770
Specific heat capacity [J/kg°C]	875
Solidus [°C]	502
Liquidus [°C]	638

The experiment is performed on a CNC milling machine, produced by Prvomajska, type AG400, 12 kW. The tool was manufactured from Cr-V-Mo tool steel (56NiCrMoV7); it has concentric circles on the shoulder and left-hand thread on the pin. The hardness of this tool after the thermal treatment (quenched and tempered condition) was 54 HRC. The material of the backing plate is steel 42CrMo4.

The temperature of the work piece during the welding is measured using a thermo-vision camera FLIR ThermaCAM P640 with the measurement range (–40 ÷ 2000 °C) and accuracy of ±2 °C. ThermaCAM Quick Report 1.1 software is used for processing the recorded data from the camera. Schematic representation of the equipment setup is given in fig. 1.

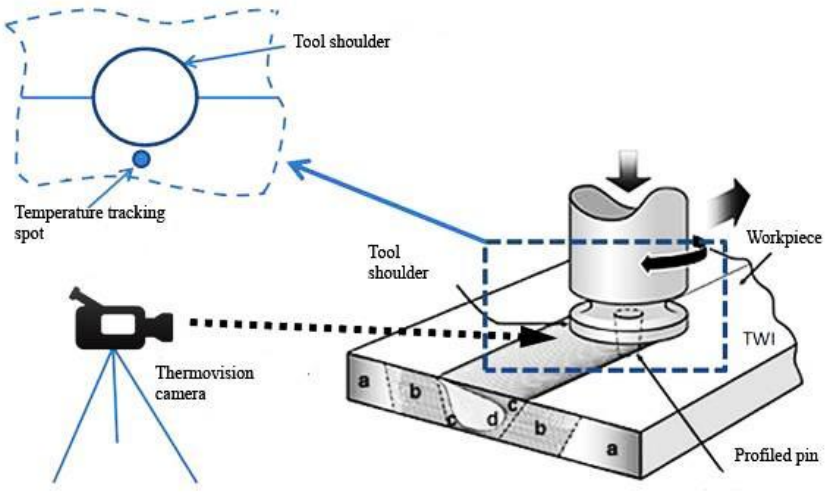

Figure 1. Schematic view of the experimental setup

Numerical model

The dimensions of the numerical model of the welding plate for the linear welding stage are 100 × 50 × 3 mm. Thermo-mechanically coupled hexahedral element with 8 nodes (C3D8RT) is used, with tri-linear displacement and temperature degrees of freedom. This element produces uniform strain (first-order reduced integration) and contains hourglass control [16]. The mesh consists of 32298 nodes and 28522 elements, while the tool (fig. 2) and the backing plate are modelled as rigid surfaces without thermal degrees of freedom. The geometry of the welding tool used in numerical analysis is given in fig. 2. The numerical model and finite element mesh for the analysis of the welding stage, as well as the modelling of the plunge stage is described in [5, 7].

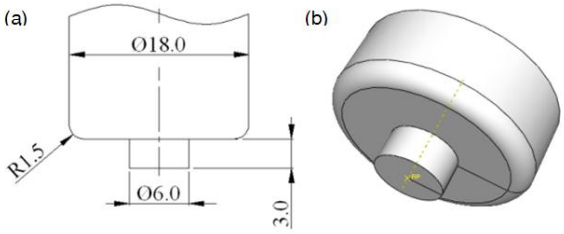

Figure 2. FSW welding tool geometry used for numerical analysis

Johnson-Cook elastic–plastic model

Johnson-Cook elastic-plastic model is an empirically based model which describes the current flow stress σ_y as a function of temperature and strain rate up to the melting point or solidus temperature [17]:

$$\sigma_y = \left[A + B(\varepsilon_p)^n\right]\left[1 + C\left(\frac{\dot{\varepsilon}_p}{\dot{\varepsilon}_o}\right)\right]\left[1 - \left(\frac{T - T_{room}}{T_{melt} - T_{room}}\right)^m\right] \tag{1}$$

where T_{melt} = 502 ºC is melting point or solidus temperature, $T_{room} = 25\,°\text{C}$ is ambient temperature, T [°C] is effective temperature, ε_p is equivalent plastic strain, $\dot{\varepsilon}_p$ is equivalent plastic strain rate, while $\dot{\varepsilon}_o$ is reference plastic strain rate. Parameters of the Johnson-Cook law for EN AW 2024 T3 are [18,19]: A = 369 MPa, B = 684 MPa, n = 0.73, m = 1.7 and C = 0.0083.

Thermal model

The heat generation during the FSW stems from two sources: frictional heating at the tool-work piece interface and plastic energy dissipation due to shearing deformation in the nugget zone [6-8]. This heat is dissipated via conduction into the work piece, the tool and the backing plate, but also by convection and radiation from the surfaces. The radiation losses are considered here as negligible because of the low temperatures; they can be combined with the convective heat transfer from the top surface of the plate by utilizing a slightly elevated heat transfer coefficient, [20]. The governing equation for heat transfer is:

$$\rho c \frac{\partial T}{\partial t} = \frac{\partial}{\partial x}\left[k_x \frac{\partial T}{\partial x}\right] + \frac{\partial}{\partial y}\left[k_y \frac{\partial T}{\partial y}\right] + \frac{\partial}{\partial z}\left[k_z \frac{\partial T}{\partial z}\right] + \dot{q}_p \tag{2}$$

where ρ is density, c is specific heat, k is heat conductivity, T is temperature, t is time, x, y, and z are spatial coordinates, while $\dot{q}_p$ is rate of heat generation due to plastic energy dissipation:

$$\dot{q}_p = \eta \tau \dot{\varepsilon}^{pl} \tag{3}$$

In eq. (3), η is factor of conversion of mechanical to thermal energy (0.9), [6, 20], τ is shear stress, while $\dot{\varepsilon}^{pl}$ is plastic strain rate. The rate of frictional heat generation $\dot{q}_f$ is:

$$\dot{q}_f = \mu p \dot{\gamma} \tag{4}$$

where μ is coefficient of friction, p is pressure and γ is the slip rate.

Heat transfer through the bottom surface of the work piece is modelled by using the heat transfer coefficient of 3000 W/m^2·K, [4, 20]. A constant value of the friction coefficient between the tool and the work piece (0.3) is assumed and the penalty contact method is used for modelling of the contact interaction. The value of the heat convection coefficient on the surface of the work piece is $h = 10\,\text{W/m}^2 \cdot \text{K}$ with the ambient temperature of 25 ºC, [4, 21].

Results and discussion

Figure 3 shows temperature field recorded by the thermo-vision camera in the 170$^{\text{th}}$ second after the beginning of the plunge stage at the fusion line, specimen 1 (plunge speed $v_{plunge} = 6$ mm/min, welding speed $v_{weld} = 40$ mm/min and rotation speed $n_{rot} = 400$ rpm) and specimen 2 (plunge speed, welding speed and rotation speed $n_{rot} = 447$ rpm). The cross marks the location on the surface of the work piece for tracking the temperature changes during the welding process. This point is located in the vicinity of the tool shoulder periphery, i.e. it is the point on the top surface of the work piece, at the distance of 12 mm from the tool symmetry axis.

A comparison of experimental and numerical results for the temperature changes during both welding stages is given in fig. 3, for the specimens 1 and 2 (the plunge stage is analysed in [5, 7]). During the experiment, heating of the gripping tool is observed, so the

starting temperature was within the range 30-60 °C for the sequence of welded specimens. This fact did not influence the welding process. When the working temperature in the welding zone has been reached, the process stabilized and the recorded temperature was between 370 and 400°C. ^{o}C

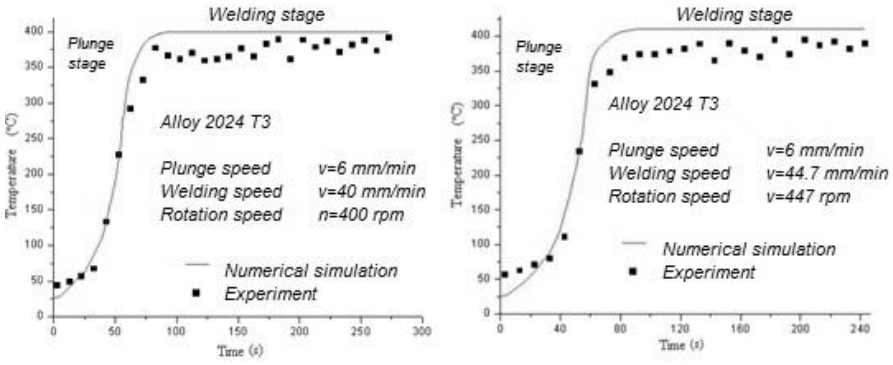

Figure 3. Dependence of temperature on time, specimens 1 and 2

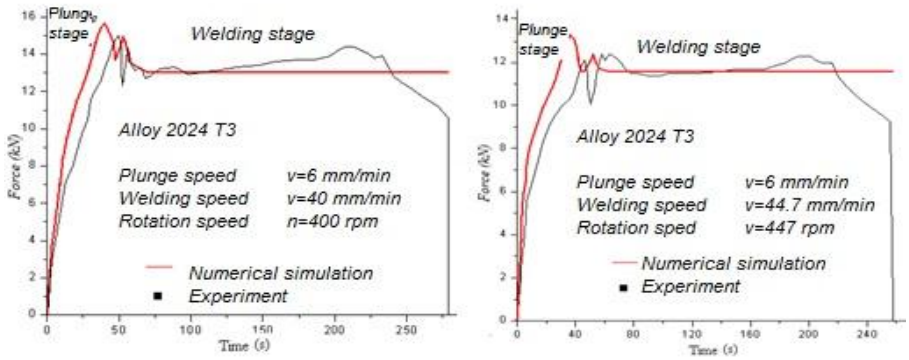

Figure 4. Dependence of force on time, specimens 1 and 2

The change of the vertical force for both welding stages (specimens 1 and 2) are shown in fig. 4. The diagrams have two characteristic jumps during the plunge stage. The first one occurs during the plunging of the tool pin, because the material has not been heated enough. After this jump, the resistance of the material is lower, because sufficient amount of heat has been generated in the region below the tool pin; this is registered on the diagram as the force drop. The second jump occurs at the moment when the tool shoulder establishes the contact with the material which is heated, but insufficiently for so large contact surface. For the plunging stage, experimental curve is slightly tilted to the right, due to the elastic deformation of the table, and it also exhibits less pronounced jump due to the thread on the tool pin. During the linear welding stage, a smaller jump of the force values is obtained during the periods when the tool passes close to the gripping positions. In the paper [22], this is explained by the fact that the working plates in the vicinity of these tools exhibit somewhat higher resistance to the tool movement. This is also a possible explanation for the force drop

which occurs when the tool comes across the free end of the working plate at the end of the welding process. The numerical results deviate from the experimental ones about 5-10%, which is sufficient for the confirmation of validity of the numerical model.

Temperature fields on the cross section of the working plate, after 12 s, are shown in fig. 5. This corresponds to the start of the second stage of the FSW process - movement of the tool along the welding line. The working plate is cut along the *x* axis and the points T1-T4 are marked; these points were used for temperature tracking during the welding process. The temperature of the plate under the tool shoulder is 430-502 ºC. Since the temperature of hot plastic working has been reached in the material under the tool, the tool can start its translation movement along the joining line without the risk of occurrence of voids or tunnels [1]. In the numerical model, this movement of the tool is represented by the flow of the material around the tool. When the temperatures in some region of the contact surface (tool shoulder - working plate) reach the melting temperature - solidus temperature (502 ºC), material has no resistance to deformation. This means that the shearing yield stress is zero; hence the heat cannot be generated by plastic deformation or friction. Therefore, the material will solidify, shearing yield stress will increase, and the conditions for heat generation by both mechanisms will be re-established. This process enables approximately constant temperatures under the tool shoulder during the welding [23]. Comparison of the temperature scale and temperature field in the first and the second image in fig. 5 reveals that the temperature on the top side of the working plate under the tool shoulder has reached 502 ºC (503 ºC is reached only in very narrow regions), which confirms the previous explanation.

The temperature field on the top surface of the working plates after 12 seconds is shown in fig. 6. The welding speed is 40 mm/min and the tool rotation speed is 400 rpm. At the beginning of welding, the temperature fields are concentric with respect to the tool axis. When the tool starts its translation along the joining line, temperature gradient of the leading side becomes larger in comparison with the trailing side; hence the temperature fields during the welding are spread behind the tool towards the trailing side. Therefore, the temperature fields are only symmetric with respect to the joining line [23]. It can be seen that the temperatures in the welding zone did not significantly change, *i. e.* maximum temperatures reached during the plunging of the tool into the plate are maintained during the welding stage. This confirms that the FSW is a repeatable process of joining in the solid state.

The temperature field in the cross-section of the working plate along the welding line (after 12 s) is given in fig. 7.

The change of temperature in the points T1-T4, for different FSW welding parameters, is given in fig. 8. As the tracking location is moved from T1 to T4, the heat source is getting closer; hence the characteristic temperature in the plunging stage is reached sooner.

During the welding stage, the temperature of the point T1, which is the farthest from the heat source, is gradually increasing. However, at the end of the simulation, when the heat generation rate is nearly constant [23], so is the temperature in T1. The point T2 is located close to the tool shoulder and its temperature is around 400 ºC. After 9 seconds, when the welding stage is stabilized, this temperature is nearly constant.

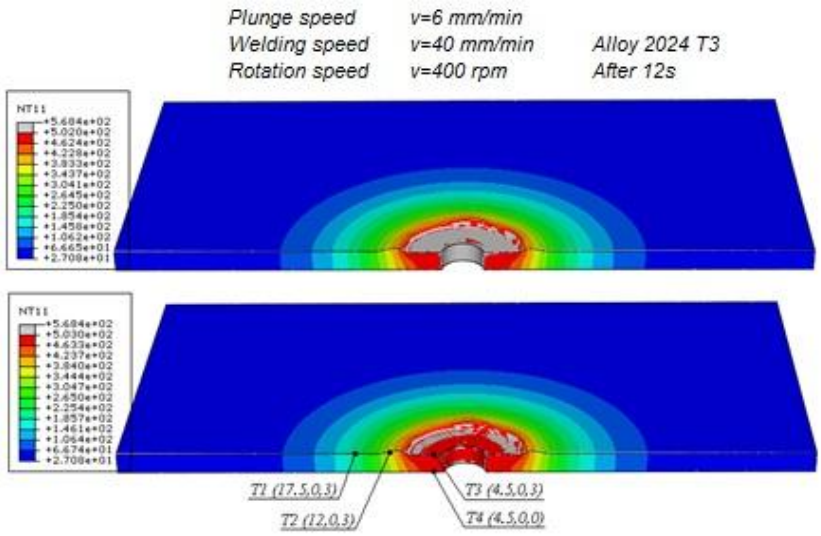

Figure 5. Temperature field after the plunging stage, at the beginning of the welding stage

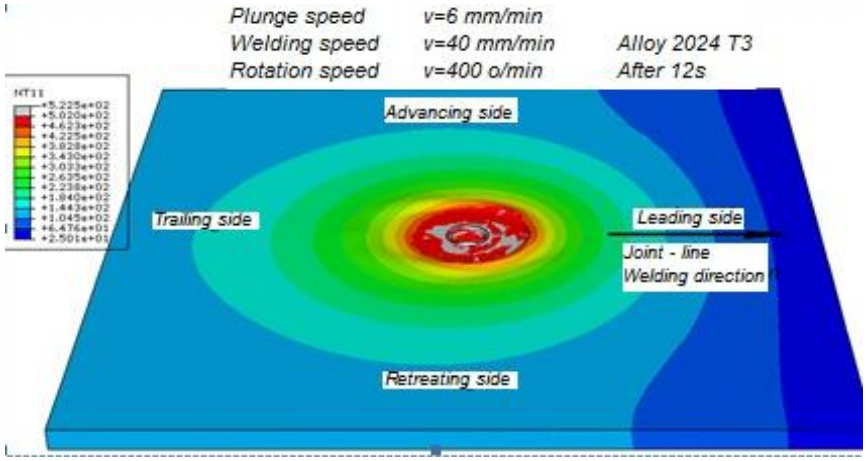

Figure 6. Temperature field on the top side of the working plate, after 12 s of welding

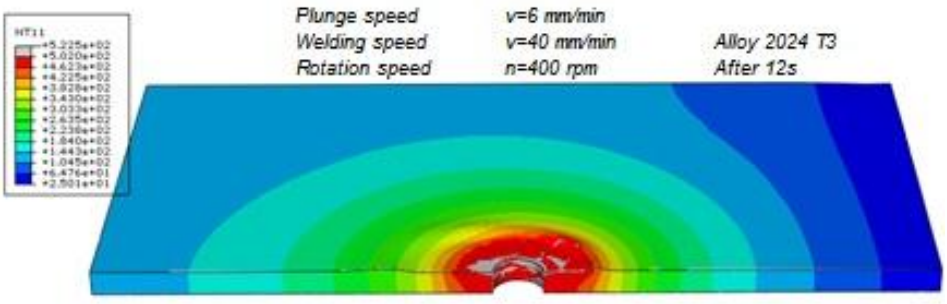

Figure 7. Temperature field after 12 s of welding, cross section along the welding line

Temperatures in the welding zone, in the points T3 and T4, are reached very early and remain constant during the entire welding process. The difference between the top and bottom surface in the welding zone is very small, 10-15 ºC. This difference decreases with the increase of distance from the heat source, and it vanishes at the distance 2*d* (*d* – diameter of the tool shoulder) from the tool axis. It can be concluded that the temperatures in T3 and T4 are the same for all the used welding parameters (of course, this is true only for the optimum values of these parameters).

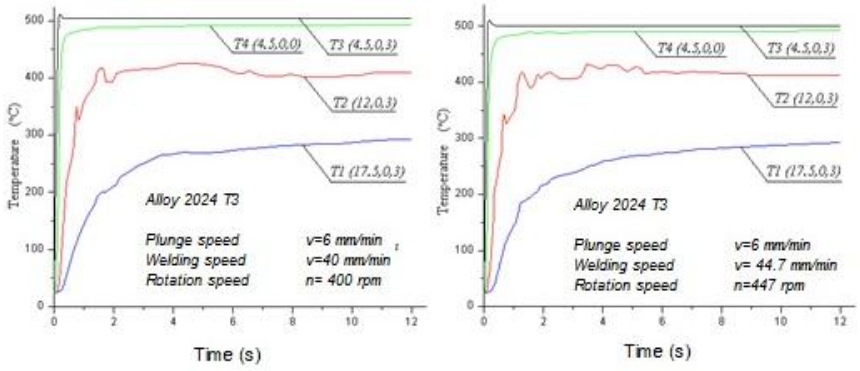

Figure 8. Dependence of temperature on time in the points T1-T4

Conclusions

The most important findings of the presented study can be summarized as follows:

- The temperature fields are symmetrical with respect to the welding line.
- The temperatures below the tool shoulder, i.e. in the welding zone, reached during the plunging stage, are approximately constant during the entire welding process.
- For optimum FSW parameters for 2024 T3 Al alloy, temperatures in the welding zone are within the range 430-502 °C, depending on the location of the tracking point.
- The temperatures of the material in the vicinity of the tool pin are approximately the same - around 500 ^{o}C.
- The temperature of the top surface of the working plate, outside the welding zone but close to the tool shoulder, is around 400°C.
- The difference between the top and bottom surface in the welding zone is very small, 10-15 ^{o}C. This difference decreases with the increase of distance from the heat source and vanishes at the distance of 2 diameters of the tool shoulder from the tool axis.

Acknowledgments

The authors acknowledge the financial support of the Serbian Ministry of Science under the projects TR 34018 and ON 174004

Nomenclature

A, B, C – Material parameter of the Johnson-Cook model [MPa]
c – Specific heat capacity [J/kg·°C]
d – Diameter of the tool shoulder [mm]
T – Temperature [°C]
T_{melt} – Solidus temperature [°C]
T_{room} – Ambient temperature [°C]
ρ – Density [kg/m^3]

E – Young's modulus [GPa]
h – Heat convection coefficient [$Wm^{-2}°C$]
k –Thermal conductivity [W/m·°C]
m –Material parameter of the Johnson-Cook model [-]
n_{rot} – Rotation speed of the tool [rpm]
n – Material parameter of the Johnson-Cook model [-]
p – Pressure [MPa]
$\dot{q}_f$ – Rate of frictional heat generation [J/s]
$\dot{q}_p$ – Rate of heat generation due to plastic energy dissipation [J/s]
t – Time [s]
σ_y – Current flow stress [MPa]
τ – Shear stress [MPa]
v_{plunge} – Plunging speed of the tool [mm/min]
v_{weld} – Welding speed [mm/min]
$\dot{\varepsilon}_p$ – Equivalent plastic strain rate [s^{-1}]
$\dot{\varepsilon}_o$ – Reference plastic strain rate [s^{-1}]
η – Factor of conversion of mechanical to thermal energy [-]
μ – Coefficient of friction [-]
ν – Poisson's ratio [-]

References

[1] Reynolds, A., Friction Stir Welding of Aluminium Alloys, in: *Handbook of Aluminium, Volume 2* (Eds. G. E. Totten, D. S. MacKenzie), Marcel Dekker; New York, 2003. pp. 579-700
[2] ***,"Friction-Stir-Welding-Of-Combat-Vehicles",
[3] http://www.twi.co.uk/news-events/case-studies/-257/
[4] Johnsen, M. R., Friction Stir Welding takes off at Boeing, *The Welding Journal, 78* (1999), 2, pp. 35-39
[5] ***, SAPA group, http://www.sapagroup.com/upload/fsw%20eng.pdf
[6] Veljić, D. *et al.*, Heat Generation During Plunge Stage in Friction Stir Welding, *Thermal Science* (2013) doi:10.2298/TSCI120301205V
[7] Veljić, D., Technology of Friction Stir Welding of Aluminium Alloys (in Serbian), M.Sc. thesis, University of Belgrade, Belgrade, Serbia, 2006
[8] Veljić, D. *et al.*, Numerical Simulation of the Plunge Stage in Friction Stir Welding, *Structural Integrity and Life, 11* (2011), 2, pp. 131-134
[9] Veljić, D. *et al.*, A Coupled Thermo-Mechanical Model of Friction Stir Welding, *Thermal Science, 16* (2012), 2, pp. 527-534
[10] Ivanović, I. *et al.*, Numerical Study of Transient Three-dimensional Heat Conduction Problem with a Moving Heat Source, *Thermal Science, 15* (2011), 1, pp. 257-266
[11] Perović, M. *et al.*, Friction-stir Welding of High-Strength Aluminium Alloys and a Numerical Simulation of the Plunge Stage, *Materials and Technologies, 46* (2012), 3, pp. 105-111
[12] Berković, M. *et al.*, Analysis of Welded Joints by Applying the Finite Element Method, *Structural Integrity and Life, 4* (2004), 2, pp. 75-83
[13] Song, M., Kovačević, R., Numerical and Experimental Study of the Heat Transfer Process in Friction Stir Welding, *Journal of Engineering Manufacture, 217* (2003), 1, pp. 73-85
[14] Chen, C. M., Kovačević, R., Finite Element Modeling of Friction Stir Welding - Thermal and Thermomechanical Analysis, *International Journal of Machine Tools & Manufacture, 43* (2003), 13, pp. 1319-1326
[15] ***, Certificate conformity, ALCOA International, Inc, Approved Certificate No. 47831, 1990
[16] Johnson, G. R., Cook, W. H., A Constitutive Model and Data for Metals Subjected to Large Strains, High Strain Rates and High Temperatures, *Proceedings*, 7th International Symposium on Ballistics, The Hague, The Netherlands, 1983, pp. 541-547
[17] ***, ASM International Aluminum 2024-T3 Data Sheet, http://asm.matweb.com/search/SpecificMaterial.asp?bassnum=MA2024T3
[18] ***, Dassault Systemes, Abaqus Analysis Manual, 2011
[19] Lesuer, D.R., Experimental Investigations of Material Models for Ti-6Al-4V Titanium and 2024-T3 Aluminum, Final Report, Department of Transportation, Washington DC, USA, 2000
[20] Veljić, D. *et al.*, Thermo-mechanical Modeling of Friction Stir Welding, *Proceedings*, 4th International Conference on Innovative Technologies for Joining Advanced Materials, 2010, pp. 171-176

[21] Schmidt, H., Hattel, J., A Local Model for the Thermomechanical Conditions in Friction Stir Welding, *Modelling & Simulation in Materials Science and Engineering, 13* (2005), 1, pp. 77-93
[22] Park, K., Development and Analysis of Ultrasonic Assisted Friction Stir Welding Process, Ph.D. thesis, University of Michigan, Ann Arbor, USA, 2009
[23] Arbegast, W., Application of Friction Stir Welding and Related Technologies, in: *Friction Stir Welding and Processing* (Eds. M. Mahoney, R. Mishra), ASM International, Materials Park, OH, 2007, pp. 273-308

Paper submitted: May 12, 2013
Paper revised: August 17, 2013
Paper accepted: October 23, 2013